COUPLED HYDROMECHANICAL EFFECTS IN CO_2 INJECTION

Jonny Rutqvist and Chin-Fu Tsang
Lawrence Berkeley National Laboratory
Earth Sciences Division
Berkeley, California

INTRODUCTION

Underground storage of carbon dioxide (CO_2) in permeable formations, such as deep saline aquifers, depleted oil and gas reservoirs, and coal seams, has been suggested as an important potential method for reducing the emission of greenhouse gases to the atmosphere (DOE 1999). The injection would take place at a depth below 800 m, so that the CO_2 would be within the temperature and pressure range of a supercritical fluid. As a supercritical fluid, CO_2 behaves like a gas with low viscosity but with a liquid-like density of 200–900 kg/m^3, depending on pressure and temperature. Because supercritical CO_2 is less dense than water, deep underground disposal requires a sufficiently impermeable caprock above an underground storage zone to trap the injected CO_2.

Caprock integrity and reservoir leakage is a key issue for both short- and long-term performance of geological CO_2 storage. In the short term, leakage is an important safety issue during active CO_2 injection. In the long term, leakage impacts the sequestration effectiveness of the once-injected CO_2. In general, two kinds of leakage mechanisms can be identified (Yamamoto and Takahashi, 2004):

1) Steady or slow leakage processes of buoyancy-driven gas flow at a rate that depends on formation permeability and fluid capillarity
2) Dynamic or rapid leakage processes along fluid paths created by interaction between formation and injected CO_2

For the slow-leakage mechanism, the fluid travels through the rock matrix, fractures, and abandoned boreholes present in the storage volume. The fluid path can be regarded as fixed in the short term, but may change slowly over the long term. Because of the limited toxicity of CO_2, a slow leakage of CO_2 is allowable from the viewpoint of short-term safety. However, such leakage may reduce long-term usefulness of CO_2 sequestration. The second, rapid leakage mechanism has been observed in nature, caused by external forces such as earthquakes. Such rapid changes could include a breach in a caprock caused by mechanical changes such as hydraulic fracturing or fault slip. For CO_2 sequestration, a rapid change in the geologic system may increase CO_2 leakage so significantly that it may be detrimental to both short-term safety and long-term environmental conservation.

In considering a site for CO_2 sequestration, it will be important to evaluate the effects of CO_2 storage on the formation, so as to minimize the risk of a breach occurring in the

system. First, injection of CO_2 will result in an increase in formation fluid pressure, especially around the injection source. Such a fluid pressure increase will causes locatel changes in the stress field, which, in turn, will induce mechanical deformations and possible irreversible mechanical failure in the caprock. This mechanical failure may involve shear along many of the existing fractures or creation of new fractures that reduce the sealing properties of the caprock system. Second, replacing the native formation fluid with CO_2 may cause changes in rock mechanical properties through chemo-mechanical interactions between the CO_2 and the host rock, or through desiccation fractures.

The evaluation of the breaching risk in a caprock/reservoir system involves prediction of complex coupled thermal-hydrological-mechanical-chemical (THMC) processes over a long period of time. Such predictions can be accomplished with appropriate numerical models and input data determined from laboratory and field experiments. Such evaluation should, if possible, be combined with *in situ* monitoring of system mechanical responses to the CO_2 injection. For example, 4D (time lapse) seismic monitoring and acoustic tomography can monitor fluid-induced changes in elasto-dynamic formation constants, from which the formation of a new leakage path through a caprock might be detected. A rapid opening of a new leakage path in an otherwise homogeneous cap rock is a dynamic change that could be followed by local fluid pressure changes, leading to CO_2 leakage. Inversely, any changes in fluid pressure will be accompanied by mechanical deformations, leading to potential changes in local elasto-dynamic properties. If those changes can be detected with seismic monitoring or other geophysical methods, they can be used as detectable precursors to a breach in a caprock and subsequent CO_2 leakage.

This paper presents an approach for analysis of coupled hydraulic and mechanical effects on caprock integrity and potential reservoir leakage during CO_2 injection. First, the fundamentals of relevant rock mechanical and hydromechanical phenomena in fractured porous rock are introduced. Then, a number of natural and industrial analogues relevant to caprock integrity and reservoir leakage are described. Following this, a numerical tool for the evaluation of coupled THM processes during underground CO_2 injection is presented. Finally, we demonstrate the use of this numerical tool for evaluation of caprock-integrity and reservoir leakage for hypothetical but realistic examples.

FUNDAMENTALS OF HYDROMECHANICAL INTERACTIONS IN FRACTURED ROCK

The term “hydromechanical (HM) coupling” refers to the interaction between hydraulic and mechanical processes. Various potential modes of mechanical responses in fractured and porous geological media (such as caprock) are schematically presented in Figure 1. The mechanical processes are coupled to hydraulic processes because geological media contain pores and fractures that can be fluid-filled and deformable. According to Rutqvist and Stephansson (2003), these couplings can be divided into “direct” HM couplings occurring through deformation and pore-fluid pressure changes, or “indirect” HM coupling, occurring through changes in hydraulic and mechanical properties (Figure 2). In any porous geological material, both direct and indirect coupled HM processes will

occur, and both are relevant for evaluation of the long-term performance of a CO_2 injection site.

Direct hydromechanical coupling and the theory of poroelasticity

Direct HM couplings occur through deformation and pore-fluid interactions, and include two basic phenomena (Wang 2000):

(i) A solid-to-fluid coupling that occurs when a change in applied stress produces a change in fluid pressure or fluid mass.

(ii) A fluid-to-solid coupling that occurs when a change in fluid pressure or fluid mass produces a change in the volume of the porous medium.

These two cases of direct HM couplings are shown schematically in Figure 2 and are labeled (i) and (ii). The second coupling is considered in Terzaghi's (Terzaghi, 1923) concept of effective (intergranular) stress. Terzaghi (1923) defines the effective stress, σ'_{zz}, in a geological medium, as the total vertical stress, σ_{zz}, less the pore fluid pressure, that is

$$\sigma'_{zz} = \sigma_{zz} - p \tag{1}$$

with compressive stress positive. However, the direct couplings—(i) and (ii) in Figure 2—are fully described in Biot's (1941) general theory of three-dimensional consolidation. Biot's equations for isotropic linear elastic porous media can be written in a "mixed stiffness form"(Wang 2000), as

$$\sigma_m = K\varepsilon_v + \alpha p \tag{2}$$

$$\xi = -\alpha\varepsilon_v + \frac{1}{M}p \tag{3}$$

where σ_m is the total mean stress (positive for compression), K is the usual (drained) bulk modulus, ε_v is the volumetric strain (positive for contraction), α is the Biot-Willis' coefficient (Biot and Willis, 1957), ξ is the increment of fluid content (positive for "gain" of fluid), and M is Biot's modulus. The introduction of the Biot-Willis coefficient as a factor multiplied to fluid pressure in Equation (2) signifies a modification and generalization of Terzaghi's effective stress law to:

$$\sigma'_m = \sigma_m - \alpha p \tag{4}$$

The coefficient α, which usually ranges between 0 and 1, has been measured in laboratory experiments (e.g., Nur and Byerlee, 1971) for a range of geological materials.

Equation (2) governs the elastic responses of the pore structure; Equation (3) governs pore-fluid responses. The two equations are coupled through the volumetric strain and fluid-pressure terms. Since the theory describes interaction between pore fluid and elastic responses, it has been called the theory of poroelasticity. Porosity variation with mechanical deformation and fluid pressure is implicitly included in Equations (2) and (3), since α and M depend on porosity, and ε_v can be linked to porosity variation. However, the macroscopic quantities α and M are frequently determined in laboratory experiments directly, without knowledge of the detailed pore-volume response at the microscopic level.

Direct coupled processes occur in all types of porous, deformable geological media, but some poroelastic phenomena tend to be more important in soft and low-permeability media. Because caprocks, such as mudstone, at CO_2 storage sites would need to have permeability as low as 10 nanodarcy it is expected that direct hydromechanical couplings are very relevant during CO_2 injection.

Indirect hydromechanical couplings and property changes

The direct couplings that occur through pore volume changes will also be accompanied by indirect couplings in the form of changes in mechanical and hydraulic properties. For example, a mechanically induced reduction in pore volume leads to a reduction of fluid flow capacity (hydraulic permeability), thereby impacting hydraulic processes. On the other hand, a reduction of pore volume may result in a stiffer material, as more contacts occur between neighboring grains. These changes in material properties can be considered indirect HM couplings. More generally, two basic phenomena of indirect HM coupling may be considered (Rutqvist and Stephansson, 2003):

(iii) A solid-to-fluid coupling that occurs when an applied stress produces a change in hydraulic properties

(iv) A fluid-to-solid coupling that occurs when a change in fluid pressure produces a change in mechanical properties

These phenomena are labeled (iii) and (iv) in Figure 2. Both direct and indirect coupled processes may be fully reversible. However, inelastic responses, including yielding, fracturing, or fault slip, are also possible, and these cause irreversible changes in porous and fractured media.

There are a large number of constitutive equations for describing changes in hydraulic properties with effective stress or deformation in geological media (Rutqvist and Stephansson, 2003). Such changes in a caprock may produce slight changes in diffuse leakage through a caprock system. However, without mechanical failure, the impact of permeability changes in intact rock is expected to be relatively small, for both the short and long-term behavior of a caprock/reservoir system. It is likely that only the hydromechanical mechanisms that induce deformation of pre-existing fractures or creation of new fractures—thus significantly change hydraulic permeability and water retention properties—are of importance to analysis caprock integrity associated with CO_2 injection.

Deformations in pre-existing fractures and creation of new fractures

Deformation of a pre-existing fracture can be induced by a change in the stress field acting on the fracture. The most basic responses of a fracture includes normal and shear displacement, caused by a change in normal and shear stresses, respectively. This is formulated according to Goodman (1970) as:

$$\Delta u_n = k_n \Delta \sigma'_n \tag{5}$$

$$\Delta u_s = k_s \Delta \sigma_s . \tag{6}$$

In Equation (5) Δu_n is the normal deformation of the fracture caused by a change in effective normal stress, $\Delta\sigma'_n$, with the magnitude of opening or closing dependent on the fracture normal stiffness k_n (Figure 1e). Likewise, Equation (6) describes the shear displacement, Δu_s, which depends on the shear stiffness, k_s, and the change in shear stress, $\Delta\sigma_s$ (Figure 1f). In a real fracture, the normal deformation is typically nonlinear, as shown in Figure 3a. The fracture stiffness typically increases as normal stress increases. One common feature of fracture deformation is the hysteresis effect during stress loading and unloading (not shown in Figure 3a), which is caused by processes arising from surface mismatch, sampling disturbances, or crushing of asperities (Barton et al. 1985).

If the shear stress acting on a fracture surface is sufficiently high, shear slip may be induced in the plane of the fracture. The most fundamental criterion for fault slip can be derived from the effective stress law and the Coulomb criterion, rewritten as:

$$\sigma_{sc} = \sigma_{sc0} + \mu_s(\sigma_n - p) \tag{7}$$

where σ_{sc} is the critical shear stress, σ_{sc0} is cohesion, μ_s is coefficient of shear friction, and σ_n is the normal stress (Scholz 1990). In a real fracture, the typical shear stress and shear displacements involve rapid increase in shear stress up to a peak, followed by a loss in load-carrying capacity. The shear displacement is accompanied by a shear dilation, as shown in Δu_n curves of Figure 3c. For a portion of the stress/deformation curve corresponding to elastic deformation of the fracture, there is minimum dilation. The onset of rapid dilation occurs when asperities begin to slide against each other. Rate of dilation (slope of Δu_n curve in Figure 3c) increases and reaches a maximum at the peak shear stress (Barton et al. 1985).

The shear strength of a fracture depends on normal stress, with a higher peak shear stress for a higher normal stress. This was examined by Byerlee (1978) for normal stresses up to 100 MPa, who derived the relationship

$$\frac{\sigma_{sc}^{Peak}}{\sigma_n} = 0.85\,. \tag{8}$$

Barton and Choubey (1977) studied shear behavior at engineering stress levels and developed empirical relationships that could be related to basic fracture characteristics, such as joint roughness or compressive strength of the rock walls. Using such empirical relationships, the amount of dilation (Δu_n versus Δu_s) can be calculated by the following expression:

$$\Delta u_n = \Delta u_s \tan d_{mob} \tag{9}$$

where d_{mob} is the mobilized dilation angle, which in turn depends on rock-wall compressive strength and normal stress across the fracture.

The fundamental criterion for tensile failure (or hydraulic fracturing) is that incipient fracture propagation will occur when the fluid pressure exceeds the least principal stress by an amount equal to or greater than the tensile strength of the rock:

$$p_{ct} \geq \sigma + \sigma_t\,. \tag{10}$$

More detailed analysis of fracturing may involve linear or nonlinear fracture mechanics, which has been applied in the analysis of propagation and control of hydraulic fracturing stimulations in petroleum engineering (Perkins and Kern 1961; Geertsma and Deklerk 1969).

Fracture fluid flow

As a first approximation the fluid flow along a fracture can be analyzed using the parallel plate flow concept, in which the fracture flow (Snow 1965; Louis and Maini 1970) between two plates with constant separation or aperture b is given by

$$\frac{Q^f}{\nabla h} = \frac{b^3 \rho_f g}{12\mu_f} w \tag{11}$$

where Q^f is volume flow rate for parallel plate (or fracture) of width (w), ∇h is head gradient, ρ_f and μ_f are fluid density and viscosity, respectively, and g acceleration of gravity. For a real fracture, hydraulic or effective aperture, b_h, can be defined as the parallel plate aperture b value that produces the same relationship between Q and Δh. Hence, fracture transmissivity is given by

$$T = \frac{b_h^3 \rho_f g}{12\mu_f} \tag{12}$$

The aperture b_h can therefore be back-calculated from fracture transmissivity, which can be determined in a flow test.

Fracture hydromechanical behavior as a function of normal stress

Experimental results typically show a decrease in fracture transmissivity with normal stress (Figure 3b), but with an apparent residual transmissivity, T_r, at high stress when the fracture appears to reach its compression limit. Figures 3a and c also show a size effect for normal closure. The size effect has been observed in experiments (e.g. Witherspoon et al. (1979), Barton and Bakhtar (1982)) and confirmed in theoretical studies (e.g. Neuzil and Tracy (1981) and Swan (1983)). Neuzil and Tracy (1981) attributed this size effect to a truncation of the aperture frequency distribution, implying that fewer of the largest, least-frequent flow channels would be included in a smaller sample.

Witherspoon et al. (1980) developed a modified cubic law, which they validated against laboratory experiments on artificial tension fractures in samples of granite and marble. They considered a general flow law,

$$\frac{Q}{\Delta h} = \frac{C}{f}(b)^n \tag{13}$$

where f is a friction factor that accounts for the roughness of the fracture surface, b is an apparent physical aperture and C is a constant depending on the flow-domain geometry and the properties of the fluid (e.g., $C = \rho_f g w/12\mu_f$ for parallel flow, see Equation (11)). If $n = 3$, this is a cubic law or modified cubic law, and then the apparent physical aperture is related to the hydraulic aperture as:

$$b = f^{1/3} b_h \tag{14}$$

A complete relationship between fracture transmissivity and effective normal stress can be derived by combining a fracture flow law (Equation (12)) with an equation for fracture normal closure (e.g. Equation (5)). Using this approach scientists have developed a number of empirical and theoretical models, which include logarithmic, hyperbolic, and exponential functions for describing the non-linear relationship between hydraulic aperture and the stress normal to the fracture (e.g., Walsh 1981, and Bandis et al. 1983).

Fracture hydromechanical behavior during shear slip

Laboratory measurements of hydromechanical behavior during shear have been rare because of a lack of specialized test equipment. The first comprehensive experimental study of permeability changes caused by shear was conducted by Makurat et al. (1990), who developed a coupled shear-flow test apparatus that could apply bi-axial stress. They concluded that whether the conductivity increases or decreases with shear depends on both the joint and rock properties, as well as the exact nature of the stress applied. Makurat et al. (1990) determined that decreases in hydraulic conductivity during shearing were a result of gouge production, which tended to block flow paths. The cases for increased hydraulic conductivity were modeled using a Barton-Bandis joint model, which predicted an increasing aperture with shear dilation, according to

$$b_E = b_{Ei} + \Delta u_n \tag{15}$$

where Δu_n is the dilation of the fracture obtained from Equation (9) and b_{Ei} is the initial mechanical aperture before shear. This equation overpredicted the increases in fracture permeability during shear, because it does not correct for the formation of gouge material in the fractures.

Gutierreze et al. (2000) conducted tests of stress-dependent permeability of a de-mineralized fracture in shale. The tests were conducted under varying normal stress as well as for shearing up to four millimeters. The results showed a typical nonlinear normal stress-versus-permeability relationship in which the permeability may change one or two orders of magnitude between maximum and minimum normal stress. The results indicated that fractures would never completely close even under normal stresses close to or higher than the unconfined compressive strength of intact shale. On the other hand, shearing of the fracture at a constant normal stress lower than the unconfined compressive strength of the shale caused dilation of the fracture and an order-of-magnitude increase in fracture permeability. Shearing at a constant normal stress higher than the unconfined compressive strength caused a negative dilation of the fracture and about a six-orders-of-magnitude reduction in fracture permeability. The reduced permeability results from the shear-induced gouge formation blocking the fracture aperture. However, despite being close to a six-orders-of-magnitude reduction, the fracture permeability was still about three orders of magnitude larger than the intact shale permeability.

Summary of indirect couplings and current state-the-of-art

In summary, the indirect coupling, involving changes in properties associated with fracturing and/or deformation of pre-existing fractures in an otherwise low permeability shale, is probably the most relevant processes to the study of caprock integrity and

reservoir leakage during CO_2 injection. Great progress has been made in the field of rock mechanics for developing constitutive models for coupled hydromechanical responses in rock fractures. The empirical work on constitutive models by Barton and Bandis (Barton and Choubey 1977, Bandis et al. 1983, Barton et al. 1985) has been especially important for practical applications. There is, however, a lack of data on hydromechanical behavior of fractured shale, especially related to permeability evolution during shear under various normal stress.

NATURAL AND INDUSTRIAL ANALOGS RELATED TO STUDY OF CAPROCK INTEGRITY AND RESERVOIR LEAKAGE

Many natural and industrial analogs exist for CO_2 sequestration. For studying caprock integrity and potential reservoir leakage during CO_2 injection, long term containment of pressurized gas and mechanical damage to shale-like formations are of particular interest. Below are brief discussions of these analogs and related studies.

Correlation between shear stress and permeability in fractured formations

In the last decade, investigations of the active lithospheric-plate boundary in California have shown that fractures favorably oriented for shear slip, the so-called critically stressed fractures, tend to be active groundwater flow paths (Barton et al. 1995, Barton et al. 1998, and Ferrill et al. 1999). The rationale for bulk permeability being dominated by critically stressed fractures is that most fractures in the bedrock are cemented because of water/rock chemical reactions. If shear slip occurs on a critically stressed fracture, it can raise the permeability of the fracture through several mechanisms, including brecciation, shear dilation, and breakdown of seals (Barton et al. 1995). Lately, similar correlations have been found at the KTB Scientific Drill Hole in Germany down to 7 km (Ito and Zoback 2000), and also at Äspö, Sweden, in the Precambrian rocks of the Baltic Shield deep in the Eurasian plate (Talbot and Sirat 2001). On the other hand, experience from injection experiments at the hot-dry rock geothermal sites in Soultz, France, and Rosemanowes, U.K., suggests that a pore-pressure increase of 5–6 MPa over ambient is needed to stimulate significant microseismicity (Evans et al. 1999). This indicates that under undisturbed stress and pressure conditions, the fractures would not be at the verge of shear failure. However, the observations about a possible correlation between maximum shear stress and permeability and experiences during injection at hot-dry rock sites can be useful for developing safe geological CO_2 sequestration techniques.

Overpressured sediments

Geological containment of pressurized gases over long time periods can be studied in the evolution of overpressured sediments and gas reservoirs (Poston and Berg, 1997). Mechanisms of pressure generation includes rapid sedimentation and compaction of sediments, hydrocarbon generation, and sediment diagenesis. In overpressured sediments, hydraulic fracturing through shale plays an important role. Field data indicate that overpressured sediments can experience episodic fluid expulsion into overlying layers during the evolution of the basin. In the case of tight sediments such as shale-rich materials with very low permeability, the most probable path of fluid leakage is by way of fractures through the tight formation (Gutierreze et al. 2000). The decrease in pore

pressure as the fluids are expelled through newly opened fractures may facilitate the precipitation of minerals along the fracture wall, which may eventually seal the fracture. The sealing of fractures can then start a new episode of overpressuring and fluid leakage during continued pressure buildup in the sediment. Given the evidence of leakage from overpressured reservoirs, evaluation of the potential for hydraulic fracturing, reopening of sealed fractures, or reactivation of faults associated with CO_2 injection is essential.

Geological storage of natural gas

Underground gas storage in reservoirs and rock caverns is a mature technology that has been practiced for decades. In North America, it is a typical practice to operate gas-storage reservoirs at or below the original reservoir pressure, out of concerns about caprock integrity, fracturing, faulting and gas loss. As pointed out by Bruno et al. (1998), the maximum safe operating pressure depends on several geomechanical factors, including *in situ* stresses, stresses induced by local and global changes in the reservoir, and the mechanical and hydraulic properties of the reservoir and overburden. Nagelhout and Roest (1997) performed numerical modeling of a generic underground natural gas storage facility to investigate the possibilities of fault slip in some of the new gas storage facilities in The Netherlands. This result showed that fault slip of up to 5 cm occurred during the initial depletion of fluid pressure from 300 bar to 115 bar. On the other hand, no inelastic fault slip occurred during the following simulated gas storage operations. However, the fluid pressure did not exceed the initial reservoir pressure by more than 14%. Generally, experience from underground gas storage is an important asset for development of a safe and efficient injection technology for CO_2. However, it is likely that underground injection of CO_2 will involve injection pressures that are considerably higher than the ambient formation fluid pressure, significantly higher than is practiced in underground gas-storage projects.

EDZ in tunnels through argillaceous rock formations

Damage in “shale-like formations” has been studies in the context of geological storage of nuclear waste in argillaceous formations. Damage in the “excavation disturbed zones” around tunnels caused by the formation of fracturing has been shown to induce significant anisotropy in ultrasonic velocity (Martin et al. 2003). In these damage zones two failure modes can be observed: extensional fractures parallel to tunnel walls (perpendicular to the least principal stress) and a combined tensile and shear failure of bedding planes (Alheid, 2003). The opening of fractures is always associated with an increase in permeability parallel to fractures. It is possible that a similar type of damage could occur in the caprock system during underground CO_2 injection. If the fluid pressure is increased sufficiently, hydraulic fractures may be created or shear-slip may occur on pre-existing fractures. Such fracturing and shear-slip may induce changes in the elastodynamic properties that could be detectable with seismic monitoring. The increased research efforts associated with nuclear waste disposal in deep tunnels in argillaceous formations could well lead to new insights into the hydromechanical behavior of those rocks that are likely candidates for caprock at CO_2 sequestration sites.

THE TOUGH-FLAC THM SIMULATOR

Coupled hydromechanical processes in CO_2 injection are complex and nonlinear, as discussed above. Their study requires the use of numerical modeling. In this section, we shall describe a recently developed numerical simulator used for CO_2 injection studies.

The TOUGH-FLAC simulator (Rutqvist et al. 2002) is based on a coupling of the two existing computer codes TOUGH2 (Pruess et al. 1999) and FLAC3D (Itasca Consulting Group 1997). TOUGH2 is a well-established code for geohydrological analysis with multiphase, multicomponent fluid flow and heat transport, while FLAC3D is a widely used commercial code designed for rock and soil mechanics. For analysis of coupled thermal-hydrological-mechanical (THM) problems, the TOUGH2 and FLAC3D are executed on compatible numerical grids and linked through external coupling modules, which serve to pass relevant information between the field equations solved in the respective codes (Figures 4). A TOUGH-to-FLAC link takes multiphase pressures, saturation, and temperature from the TOUGH2 simulation and provides updated temperature, and pore-pressure information to FLAC3D (Figure 4). Because the TOUGH2 mesh uses one gridpoint within each element, and FLAC3D nodes are located in element corners, data have to be interpolated from mid-element (TOUGH2) to corner locations (FLAC3D).

After data transfer, FLAC3D internally calculates thermal expansion and effective stress according to:

$$\Delta\boldsymbol{\varepsilon}^T = \mathbf{I}\beta_T \Delta T \tag{16}$$

$$\boldsymbol{\sigma}' = \boldsymbol{\sigma} - \mathbf{I}\alpha P \tag{17}$$

where $\boldsymbol{\varepsilon}^{\mathbf{T}}$ is thermal strain, β_T is the linear thermal expansion coefficient, $\mathbf{I}$ is the unit tensor, T is temperature, $\boldsymbol{\sigma}'$ is effective stress, $\boldsymbol{\sigma}$ is total stress, α is the Biot effective stress parameter, and P is pore fluid pressure. In a multiphase flow calculation, the value of P transferred to FLAC3D could represent an average pore pressure calculated from the pressures of the various phases (Rutqvist et al. 2002).

A FLAC to TOUGH link takes element stress and deformation from FLAC3D and updates element porosity, permeability, and capillary pressure to be used by TOUGH2, according to the following general expressions:

$$\phi = \phi(\boldsymbol{\sigma}', \boldsymbol{\varepsilon}) \tag{18}$$

$$\mathbf{k} = \mathbf{k}(\boldsymbol{\sigma}', \boldsymbol{\varepsilon}) \tag{19}$$

$$P_c = P_c(\boldsymbol{\sigma}', \boldsymbol{\varepsilon}) \tag{20}$$

No interpolation in space is required for this data transfer because stress and strain are defined in FLAC3D elements, which are identical to TOUGH2 elements. A TOUGH-FLAC coupling module for this link should calculate the hydraulic property changes, based on material-specific theoretical or empirical functions.

A separate batch program controls the coupling and execution of TOUGH2 and FLAC3D for the linked TOUGH-FLAC simulator. It was done within the FLAC3D input file using

the FLAC-FISH programming language (Itasca Consulting Group 1997). The calculation is then stepped forward with the transient TH analysis in TOUGH2, by conducting, at each time step or at the TOUGH2 Newton iteration level, a quasi-static mechanical analysis with FLAC3D, to calculate stress-induced changes in porosity and intrinsic permeability. Because of small strain conditions, there is no change in mesh dimension during the simulations.

APPLICATION OF TOUGH-FLAC TO CO_2 INJECTION

The TOUGH-FLAC code is applied to simulate an injection operation for disposal of CO_2 into a permeable brine formation, which is overlain by a semi-permeable caprock (Figure 5). Coupled HM interactions in a caprock/reservoir system are studied with a view towards their role on the integrity of the caprock system and reservoir leakage. This analysis is an extension of a recently published analysis of coupled hydromechanical changes in a brine-aquifer/caprock system during CO_2 injection (Rutqvist and Tsang 2002). Our present study utilizes the same model for the brine-aquifer/caprock system, but is focused on the evolution of stresses during the CO_2 injection. In particular, we are studying the role of the initial stress regimes on the potential for faulting and fracturing, in a pre-existing fracture zone, and along existing sealing faults.

In our model, we inject CO_2 at a constant rate over a 30-year period at a depth of 1,300 to 1,500 m. The injection zone is overlain by a 100-m-thick caprock, located at 1,200 to 1,300 m. Three cases of brine-aquifer/caprock systems are studied (Figure 5):

1) A brine-aquifer caprock system with no lateral confinement
2) A caprock intersected by a fracture zone which is initial hydraulically inactive
3) A brine-aquifer/caprock system with two sealing faults.

All simulations are conducted in two-dimensional vertical section models, which are extended far enough in the lateral directions to be “infinite-acting” (Figure 5). The two-dimensional geometry implies that injection take place in a well field that consist of a long line of injection wells.

Material properties

The material properties are given in Table 1. They correspond to a sandstone aquifer with a caprock of shale. Functions are developed or discussed for relative permeability, capillary pressure, and porosity-stress and porosity-permeability correlation (Rutqvist and Tsang 2002).

Isotropic hydromechanical rock properties are represented by a porosity-mean stress and a permeability-porosity relationship. The porosity, ϕ, is related to the mean effective stress as

$$\phi = (\phi_0 - \phi_r)\exp\left(-5 \cdot 10^{-8} \cdot \sigma'_M\right) + \phi_r \tag{21}$$

where ϕ_0 is porosity at zero stress, ϕ_r is residual porosity at high stress, and the mean effective stress (in Pa) is defined from the principal stresses as

$$\sigma'_M = \frac{1}{3}\left(\sigma'_1 + \sigma'_2 + \sigma'_3\right) \tag{22}$$

The effective principal stresses (with compression positive) are calculated (Rutqvist et al. 2002) as follows:

$$\sigma'_1 = \sigma_1 - \alpha\overline{P} \tag{23}$$

$$\sigma'_2 = \sigma_2 - \alpha\overline{P} \tag{24}$$

$$\sigma'_3 = \sigma_3 - \alpha\overline{P} \tag{25}$$

where α is Biot's effective stress parameter and $\overline{P}$ is an average pore pressure defined for an unsaturated system as:

$$\overline{P} = S_l P_l + \left(1 - S_l\right)P_g \tag{26}$$

In the current calculations, we have put α = 1, which is a reasonable value. The permeability is correlated to the porosity according to the following exponential function (modified from Davis and Davis, 1999):

$$k = k_0 \exp\left[22.2\left(\phi/\phi_0 - 1\right)\right] \tag{27}$$

where k_0 is the zero-stress permeability.

The coefficients in the functions for porosity and permeability changes (Equations (27) and (25)) are obtained by matching to laboratory measurements on sandstone presented by Davis and Davis (1999). Their experimental data show a one-order-of-magnitude reduction in permeability with effective stress increasing from zero to 30 MPa. In addition to the two coupling functions in Equations (21) and (27), the capillary pressure is also modified according to a function due to Leverett (1941):

$$P_c = P_{c0}\left(S_l\right)\frac{\sqrt{k_0/\phi_0}}{\sqrt{k/\phi}} \tag{28}$$

Thus, porosity, permeability, and capillary pressure are all directly or indirectly dependent on the mean effective stress. In this analysis, the relationships for porosity as a function of stress and for permeability as a function of porosity—derived for sandstone—are also used for the shale. However, for the shale, the flowing porosity and permeability are assumed to be two to four orders of magnitude lower than for sandstone. Note that total porosity of shale can be much greater than the porosity given in Table 1, which is the connected porosity available for fluid flow.

In our modeling, we will analyze the possibilities of a failure of the caprock by looking at the critical pressure that could induce hydraulic fracturing or the critical pressure that could induce shear slip of pre-existing faults. A conservative assumption is that a hydraulic fracture could develop as soon as the fluid pressure exceeds the least compressive principal stress, and hence, the critical pressure for fracturing derived from Equation (10) is:

$$P_{fc} = \sigma_3 \tag{29}$$

A conservative assumption for the onset of fault slip is that it is the condition under which a fault could exist at any point with an arbitrary direction. For such a case, the Coulomb failure criterion can be written in the following form (Jaeger and Cook 1979):

$$\left|\tau_{m2}\right| = -\left(\sigma_{m2} - P_{sc}\right)\sin\varphi + S_0 \cos\varphi \tag{30}$$

where τ_{m2} and σ_{m2} are the two-dimensional maximum shear stress and mean stress in the plane σ_1, σ_3, defined as:

$$\tau_{m2} = \frac{1}{2}\left(\sigma_1 - \sigma_3\right) \tag{31}$$

$$\sigma_{m2} = \frac{1}{2}\left(\sigma_1 + \sigma_3\right) \tag{32}$$

and S_0 and φ are the faults coefficient of internal cohesion and angle of internal friction, respectively.

For faults, a zero cohesion may be assumed, and a typical range for φ is 25° to 35° (Goodman 1989). In the following calculations, we test for slip using a zero cohesion (S_0 = 0) and a friction angle of 30°.

Initial and boundary conditions

At the start of the CO_2 injection operation, the initial temperature and pressure at the injection point (about 1,500 m depth), are T = 47.5 °C and P = 15.1 MPa, respectively (see Table 2). This is well within the range for assuring a supercritical CO_2. At this depth, the initial stress is $\sigma_v = \sigma_h$ = 33.2 MPa (for isotropic initial stress case), and the initial mean effective stress is 18.1 MPa, leading to a permeability of about 0.3×10^{-13} m^2 (~30 millidarcy) in the aquifer and 0.3×10^{-17} m^2 (~3 nanodarcy) in the caprock.

As mentioned above, the lateral boundaries are placed far away from the injection points, and therefore the model can be considered as infinite in its lateral direction. At the bottom, roller boundaries (no displacement normal to the boundary) and a constant temperature of 85°C is maintained throughout the simulation. This simulation is conducted in an isothermal mode, which implies that the thermal gradient is maintained according to the initial conditions throughout the simulation.

CO_2 injection

Compressed CO_2 is injected at a constant rate of 0.05 kg/s per meter (normal to the two-dimensional model). With such an injection rate, the aquifer pressure increases substantially with time, and after several years of injection, the pressure would exceed the lithostatic stress of 33.2 MPa. Considering the amount of CO_2 that would have to be disposed from a single coal-fired power plant, a high pressure increase would be expected. For example, a standard size 1,000 MW coal-fired power plant that produces CO_2 at a rate approximately 350 kg/s (Hitchon, 1996) would require a well field about 7 km wide (0.05 kg/s per meter ×7,000 m = 350 kg/s). An axisymmetric simulation conducted by Pruess et al. (2001) for this injection rate (350 kg/s) into a 1 km diameter

well field leads to a pressure increase of about 17 MPa, which is very similar to what we obtain in our two-dimensional modeling with an injection rate of 0.05 kg/s per meter.

Evolution of fluid pressure and spread of CO_2

Figure 6a presents the calculated injection pressure during a 30-year injection period, with or without consideration of the stress-dependent rock-mass permeability. The difference in injection pressure is explained by permeability in the injection zone increasing, in the former case, because of a general reduction in effective stresses. However, these changes in permeability are moderate (less than a factor of 2) because of a rather insensitive stress-permeability relationship for porous sandstone.

Figure 6b presents the spread of CO_2 fluid and fluid pressure within the aquifer/caprock system after 10 years of injection for the HM calculation. The figure shows that the CO_2 has spread under the cap over 4 km and has penetrated upwards into the caprock by about 10 m. At this time the, injection pressure has increased to 33 MPa, which is slightly less than the lithostatic stress at the injection point (Figure 6a).

Figure 7 presents the evolution of fluid pressure, CO_2 gas saturation and permeability along a vertical profile at the injection point (x = 0). The figure shows that although fluid pressure is approximately equal to the lithostatic stress at the injection point (at about 1,450 m), the fluid pressure actually exceeds the lithostatic stress at the lower parts of the caprock. However, even though the fluid pressure is close to or even exceeds the lithostatic stress, changes in permeability are relatively small. This is because these changes in permeability depend on changes in the effective mean stress, which in turn depends on stress changes in both the horizontal and vertical direction. As will be described in more detail below, poroelastic compressive stresses can build up and provide increased confining stresses, especially in the horizontal direction. These injection-induced increases in confining stresses tend to prevent large changes in effective stress, which in turn prevent large permeability changes.

Evolution of injection-induced (poroelastic) stress changes

Figures 8 and 9 show how hydraulic injection causes changes in both confining and effective stresses in the caprock/reservoir system. These local changes in the stress field are caused by complex poroelastic responses as CO_2 fluid is added to the system. Figure 8 indicates that the vertical and horizontal *in situ* stresses (total stresses) increase near the injection point. The stresses increase as a result of poro-elastic stresses that occur when the porous rock attempts to expand in a confined rock mass. Both vertical and horizontal stresses increase in the injection aquifer. However, in the caprock, just above the injection interval, the horizontal stresses increase much more than the vertical stresses. Figure 9 presents changes in vertical and horizontal effective stresses near the CO_2 plume. The figure shows that the effective stresses are reduced mostly at the interface between the injection aquifer and the caprock, and the vertical effective stress is reduced more than the horizontal one.

Potential for shear slip and fracturing at different stress regimes

The injection-induced incremental stresses caused by poroelastic responses (shown in Figures 8 and 9) are independent of the initial stress field as long as the rock behaves elastically. However, if the induced stress changes are sufficiently large, or if the fluid pressure exceeds the confining stresses, inelastic mechanical yielding failure may occur. In this case, the potential for rock-mass failure is governed by the evolution of the magnitude and directions of maximum and minimum principal effective stresses and their relation to critical stresses, defined in the adopted failure criteria (Equations 29 and 30).

Figure 10 presents vertical profiles of the evolution of fluid pressure, and vertical confining (total) and effective stresses. The vertical effective stresses are reduced most at the interface between the injection zone and the caprock (at 1300 m). At this location there is a relatively large increase in fluid pressure, but a relatively small increase in confining stress. However, note that even though the fluid pressure exceeded the lithostatic stress in the lower part of the caprock and over most of the injection zone, the effective vertical stress is still in compression. As a result, no hydraulic fracturing is expected.

Figures 11 and 12 presents vertical profiles of the evolution of horizontal confining and effective stresses for two different stress regimes:

1) An isotropic stress regime ($\sigma_h = \sigma_v$)
2) A reverse fault stress regime ($\sigma_h = 0.7\sigma_v$)

Figure 11 indicates that the horizontal effective stress is well into the compression at all times, and therefore formation of vertical hydraulic fractures is highly unlikely. Comparing the evolution of horizontal stresses in Figure 11 with the evolution of vertical stress in Figure 10 again illustrates that the vertical effective stresses change much more than the horizontal effective stresses. As discussed above, the reason is that poroelastic stresses develop more strongly in the horizontal direction than the vertical direction, which helps to offset the effects of increasing fluid pressure. Comparing the vertical profiles of effective stress evolution in Figure 11 (for isotropic stress regime) with those in Figure 12 (for reverse faulting stress regime) demonstrates the great importance of the initial (pre-injection) horizontal stress magnitude. Figure 12 shows that the local horizontal effective stresses become very close to tensile at the interface between the caprock and injection zone (1,300 m). This implies that for the case of a reverse faulting stress regime, there is an increased likelihood for formation of vertical fractures at this location.

Figures 13 and 14 show the zones of possible fault slip and hydraulic fracturing for the two cases of stress regime. The potential for hydraulic fracturing and fault slip was evaluated using Equations (29) and (30). Figure 13 indicates that for the isotropic stress regime, mechanical failure would most likely initiate at the interface between the caprock and injection the zone. In this zone, the reduction in vertical effective stress can lead to the formation of horizontal hydraulic fractures (Figure 13b). Furthermore, a larger zone of possible slip on pre-existing fractures occurs at the upper and lower part of the injection zone. This finding implies that an unfavorably oriented fault could be

reactivated with accompanying micro-seismicity and possible permeability change. However, even if fracturing or fault reactivation would take place in the lower parts of the caprock, the simulation indicates that it would be contained within the lower part of the cap and would not propagate through the upper part of the cap.

Figure 14 shows that, for the reverse faulting stress regime, the zones of potential shear slip and hydraulic fracturing are more extensive. This is because in this case the initial, far-field horizontal stress is lower. Importantly, in the case of a reverse faulting stress regime, shear slip and hydraulic fracturing would preferentially occur on vertical fractures. Further, the shear slip could occur in the entire caprock and not just in its lower part. Thus, there would be a potential for slip of a pre-existing fault crossing the entire caprock with a potential for leakage.

Effect of a vertical weakness zone in the cap

A weakness is introduced into the caprock in the form of a 10-m wide vertical fracture zone (Figure 15). The fracture zone is simulated as a porous medium, more porous than the surrounding caprock, with a much more sensitive porosity-stress relationship (Table 1). The fracture zone is initially assumed to have the same permeability as the surrounding caprock (Table 2). Thus, the fracture zone could be envisioned as consisting of closely spaced fractures that have been healed and are completely closed (from the hydraulic point of view). The fractures in this zone have no tensile strength and can thus open up as a result of a reduction in effective stress when fluid pressure increases.

Using the assumed sensitive stress-versus-permeability function, the fault permeability increases as the fluid pressure increases within the caprock. As a result, CO_2 starts to leak at the top of the caprock after about 6 years of injection (Figure 15). As the pressure increases during the CO_2 injection, the effective stresses are reduced in the fault, and consequently the fault tends to open for more flow, according to the assigned stress-porosity-permeability relationships (Equations (21) and (27) and Table 1). In this simulation, the permeability of the fault increases gradually up to two orders of magnitude during the first 10-year period of the injection. Consequently, the brine could more easily be displaced upwards through the fault by the less-dense CO_2 fluid. At 10 years, the CO_2 has broken through the cap and is slowly leaking and migrating upwards by buoyancy (Figure 15, left). However, at 10 years, the increase in the leakage rate is only about 6% of the injected CO_2, and therefore the leakage cannot be detected by monitoring the evolution of injection pressure. As described by Rutqvist and Tsang (2002), the leakage rate through the fracture zone accelerates at about 5.7 years (Figure 15, right) due to several contributing factors, including changes in relative permeability, fluid viscosity and fluid pressure-induced fracture opening, as the fracture zone is invaded by CO_2.

The evolution of the stress field in the aquifer/caprock system is similar to that of the homogenous caprock case (Figures 8 and 9), except for the evolution of stresses in the fracture zone itself. This is illustrated in Figure 16, which shows the evolution of fluid

pressure, confining stress, and effective stresses along two vertical profiles through the caprock:

1) A vertical profile through the caprock along the vertical fracture zone at x = +75 m
2) A vertical profile through intact caprock at x =-75 m.

The figure indicates that fluid pressure in the vertical fracture zone (in upper part of the caprock, at 1,200 m) significantly increases compared to the case of an intact caprock. The higher permeability in the fracture zone implies that fluid pressure can penetrate upward more rapidly than in the surrounding low-permeability intact rock. Furthermore, almost no difference exists in the confining stress within the fracture zone. This is explained by the fact that poroelastic stresses in the caprock result form the overall fluid pressure increases over a wide lateral dimension, whereas a local fluid pressure change within a narrow fractures zone will not give rise to significant poroelastic stresses. Instead, the invaded fluid pressure will tend to reduce the effective stresses within the fracture zone, with the effect of a local expansion and opening of pre-existing fractures in the fracture zone. The simulation results for the case of a reverse stress regime indicates that the fluid pressure increases in the fault would be sufficiently high to change the horizontal effective stresses to tension. A reduction of horizontal effective stresses along the fracture zone implies that pre-existing fractures could be completely unloaded and propagated to provide additional connectivity for fluid flow through the fracture zone (Figure 17).

Injection into a reservoir/caprock system bounded by two sealing faults

The TOUGH-FLAC code can simulate slip explicitly along major faults through constitutive mechanical models and slip line elements available in FLAC3D. Figure 18 shows an example of fault reactivation analysis using this model. In this example, CO_2 is injected within a permeable injection zone laterally confined between two sealing (low permeability) faults. The material properties of the injection zone and caprock are those given in Table 1. An internal friction angle of 25° is assumed for the faults. In this case, CO_2 was injected at high pressure until slip was triggered along the two bounding faults. A maximum fault slip of about 5 cm was predicted along fault sections intersecting the injection zone (Figure 18, right). However, analysis shows that shear failure is limited to a zone of substantially increased fluid pressure and does not propagate further than about 100 m above and below the injection zone. In general, the stress evolution around the faults and the injection zone is more complex in this case than for the homogenous caprock case. Localized concentration of stresses (including shear stresses) as well as localized stress releases are more likely, and this could lead to additional damage, particularly in areas where the fault intersects the caprock. Such damage may induce increased permeability along the fault. However, this possibility was not considered in this initial study.

In general, slip on pre-existing faults and other discontinuities which intersect the caprock are viewed as a likely scenario for generation of possible leakage paths for CO_2. However, further analysis is required to evaluate whether or not fluid flow will occur in conjunction with the slip. Shear test on single fractures in shale indicates that

permeability can increase or decrease depending on the current stress normal to the fractures (Gutierrez et al. 2000). At high normal stresses, shear slip is accompanied with significant gouge production, and the permeability can actually decrease by several orders of magnitude. However, geological studies indicate that local stresses and the presence of faults control containment and release of deep overpressured fluids. Further research is needed for a realistic modeling of complex fault structures and for modeling of potential changes in fault permeability and mechanical properties.

DISCUSSION AND CONCLUSIONS

Given that this is a general presentation of coupled hydromechanical changes during a CO_2 disposal operation, the analysis is somewhat simplified. Because of a lack of field data, some of the properties used in our simulations have been estimated. As such, results of this study should be taken only qualitatively, since the quantitative results are very sensitive to the assumed rock properties. At a real injection site, the parameters for these empirical relationships should be calibrated against *in situ* measurements at an appropriate scale, and over an appropriate range of values.

The analysis provided in this report focuses on the evolution of injection-induced stresses in the caprock and the potential for inducing mechanical failure that could be detrimental to the performance of a CO_2 injection operation. A simplified failure analysis is conducted, based on the evolution of induced effective stress changes for three cases of initial *in situ* stresses. Results indicate that the most important process in hydromechanical behavior of the caprock is a general reduction of the mean effective stress, caused by the high-pressure injection of CO_2. The largest reduction of mean stress was found at the interface between the injection zone and caprock, and in the lower parts of the caprock. This reduction of mean stress is not only important for permeability changes and hydraulic fracturing, but is also very important for a potential initiation of shear slip. It results in a lower shear strength at the same time when the shear stress is somewhat increased. In combination, these effects increase the possibility of shear failure.

The analysis also shows that it is very likely that an onset of shear failure would occur prior to any hydraulic fracturing. This is partly a consequence of the slow increase in fluid pressure over the 10-year injection period. When the pressure increases slowly, fluid has the time to diffuse into the neighboring rock formation, which then expands and locally increases the total stress. Because of the geometry of the extensive horizontal aquifer, total stresses increase more in the horizontal than in the vertical direction. This has two consequences: First, it will prevent reduction of effective stress in the horizontal direction and thereby prevent the formation of vertical hydraulic fractures. Secondly, because the total stresses increase more in the horizontal direction, the maximum principal stress, σ_1, will tend to become horizontal, and the difference between σ_1 and σ_3 (a measure of shear stress) will increase.

An important result of this analysis is the observation that the induced hydraulic fracturing and shear reactivation could be contained within the lower portion of the

caprock. Thus, the sealing mechanism of the caprock may still be functioning in the upper part. The reason for this continued functioning is that the mean stress does not change very much in the upper part of the caprock, because the fluid pressure at that location is mostly controlled by the constant hydrostatic pressure in the upper permeable formation above the caprock. In the case of a vertical fault, it can also be observed that most of its permeability changes occur in the lower part of the caprock, while the opening of the fault was much smaller in the upper part. All these observations indicate that the upper part of the caprock can act as a bottleneck for CO_2 migration through the caprock. Once the CO_2 reaches the upper exit of the fault, the upward CO_2 migration will accelerate because of both hydraulic and hydromechanical changes. Further, if a more rapid invasion of CO_2 and fluid pressure occurs through a permeable fracture zone, the effective stresses would change more dramatically in this zone compared to the surroundings. The local reduction in effective stress may reopen fractures within this fracture zone, and if pressure is sufficiently high, fracturing could occur.

The analysis also shows that the magnitude and anisotropy of the initial stress field is an important factor in determining when and how failure could occur. In the case of an isotropic stress field, with both stresses equal to the weight of the overburden, shear slip along low-angle faults and the formation of horizontal hydraulic fractures are the most likely failure modes. In the case of relative low horizontal stress (which might be the most common case in these types of formations), shear slip along steep faults and formation of vertical fractures are the most likely failure modes.

In summary, the following points on coupled hydromechanical effects in CO_2 injection may be highlighted:

- A general reduction in the effective mean stress induces strongly coupled hydromechanical changes in the lower part of the caprock. Therefore, the strongest hydromechanical changes and the greatest risk of rock failure occur in the lower part of the caprock.
- Because the aquifer pressure slowly increases during the injection period, fluid has time to diffuse into the rock and create poroelastic stresses. These events will decrease the probability of fracturing and shear, but also make the shear reactivation more likely. Thus shear reactivation of existing fractures is the primary failure mode of concern in CO_2 injection.
- The analysis indicates that shear reactivation in the lower part of the caprock could take place at an injection pressure well below the lithostatic pressure. However, depending on the initial *in situ* stress field, this fault slip reactivation may or may not be confined to the lower parts of the caprock.
- The type of stress regime (e.g., isotropic or reverse fault types) is a key parameter that determines whether fracturing and shear slip are likely to take place along subhorizontal or subvertical fractures. For a common reverse fault type of stress regime, fracture slip would preferentially take place along subvertical fractures, so that hydraulic fracturing would be vertical.

- Once the CO_2 fluid reaches the upper part of the caprock (for example through a permeable fault) the upward CO_2 migration is accelerated because of the combined effects of relative permeability and viscosity changes, as well as changes in intrinsic permeability caused by pressure-induced hydromechanical effects.

ACKNOWLEDGMENTS

Review and comments by Dr. Christine Doughty and Dr. Kurt Nihei at the Lawrence Berkeley National Laboratory are much appreciated. We gratefully acknowledge the support by the Office of Science, Office of Basic Energy Sciences, Chemical Sciences and Geosciences Division of the U.S. Department of Energy, under contract No. DE-AC03-76SF00098.

REFERENCES

Alheid H.-J. (2003). Lessons learned in indurated clays. In: Impact of Excavation Disturbed or Damaged Zone (EDZ) on the Performance of Radioactive Waste Geological Repositories. Proceedings of a European Commission CLUSTER Conference, Luxembourg, November 3–5, 2003.

Bandis S, Lumsden A C and Barton N R (1983) Fundamentals of rock joint deformation. Int J Rock Mech Min Sci & Geomech Abstr 20:249-268.

Barton C A, Hickman S H, Morin R and Zoback M D (1998) Reservoir-scale fracture permeability in the Dixie Valley, Nevada, Geothermal fields. Society of Petroleum Engineers, SPE Paper no 47371.

Barton C A, Zoback M D and Moos, D (1995) Fluid flow along potentially active faults in crystalline rock. Geology 23:683-686.

Barton N R and Bakhtar K (1982) Rock joint description and modeling for the hydrothermomechanical design of nuclear waste repositories. Technical Report 83-10, TerraTek Engineering, Salt Lake City, Utah.

Barton N R, Bandis S and Bakhtar K (1985) Strength, deformation and conductivity coupling of rock joints. Int J Rock Mech Min Sci & Geomech Abstr 22:121-140.

Barton N and Choubey V (1977) The shear strength of rock joints in theory and practice. Rock Mech 10:1-54.

Biot M A (1941) A general theory of three dimensional consolidation. J Appl Phys 12:155-164.

Biot M A and Willis D G (1957) The elastic coefficients of the theory of consolidation. J Appl Mech 24:594-601.

Bruno M S, Srinivasa MM, Danyluk PM, Hejl K A and Anduisa J P (1998) Fracture injection of solid oilfield wastes at the West Coyote field in California. In: EUROCK '98, Rock Mechanics in Petroleum Engineering, Society of Petroleum Engineers, SPE Paper no 47371.

Byerlee J D (1978) Friction in rocks. J Pure Appl Geophys 73:615-626.

Corey A T (1954) The interrelation between oil and gas relative permeabilities. Producers Monthly November 1954: 38-41.

Davis J P and Davis D K (1999) Stress-dependent permeability: characterization and modeling. Society of Petroleum Engineers, SPE Paper no 56813.

DOE (1999) Carbon Sequestration Research and Development, D. Reichle and others (eds.), U.S. Department of Energy Report DOE/SC/FE-1, Washington, DC.

Evans KF, Cornet FH, Hashida T, Hayashi, K, Ito T, Matsuki, K, Wallroth T (1999) Stress and rock mechanics isssues of relevance to HDR/WDR engineered geothermal systems: review of developments during the past 15 years. Geothermics 28:455-474.

Ferrill D, Winterle J, Wittmeyer G, Sims D, Colton S and Armstrong A (1999) Stressed rock strains groundwater at Yucca Mountain, Nevada. GSA Today, Geological Society of America, May 1999.

Geertsma J and Deklerk F (1969) A rapid method of predicting width and extent of hydraulically induced fractures. J Pet Tech 21:1571-1581.

Goodman R E (1970) Deformability of joints. In: Symposium on Determination of the In-Situ Modulus of Deformation of Rock, ASTM, S T P 477, pp. 174-196.

Goodman R E (1989) Introduction to Rock Mechanics. Second edition. John Wiley & Sons, New York, USA.

Gutierreze M., Oino L.E., and Nygård (2000) Stress-dependent permeability of a de-minerarised fracture in shale. Marine and Petroleum Geology 17:895–907.

Hitchon B (1996) Aquifer Disposal of Carbon Dioxide. Geoscience Publishing Ltd, Sherwood Park, Alberta, Canada.

Itasca Consulting Group (1997) FLAC 3D, Fast Lagrangian Analysis of Continua in 3 Dimensions. Version 2.0. Five volumes. Minneapolis, Minnesota: Itasca Consulting Group.

Ito T and Zoback M D (2000) Fracture permeability and *in situ* stress to 7 km depth in the KTB scientific drillhole. Geophys Res Let 27:1045-1048.

Jaeger J C and Cook N G W (1979) Fundamentals of Rock Mechanics. Chapman and Hall, London.

Leverett M C (1941) Capillary behavior in porous media. Trans AIME. 142: 341-358.

Louis C and Maini Y (1970) Determination of *in situ* hydraulic parameters in jointed rock. In: Proc 2nd International Congress on Rock Mechanics, Vol I, pp 235-245.

Makurat A, Barton N and Rad N S (1990) Joint conductivity variation due to normal and shear deformation. In: Barton N and Stephansson (eds) Rock Joints pp 535-540.

Martin C.D., Lanyon G.W., Blumling P., and Mayor J.C. (2003) The excavation disturbed zone around a test tunnel in the Opalinus Clay. In: Impact of Excavation Disturbed or Damaged Zone (EDZ) on the Performance of Radioactive Waste Geological Repositories. Proceedings of a European Commission CLUSTER Conference, Luxembourg, November 3–5, 2003.

Nagelhout A C G and Roest J P A (1997) Investigating fault slip in a model of underground gas storage facility. Int J Rock Mech Min Sci & Geomech Abstr 34:Paper no 212.

Neuzil C E and Tracy J V(1981) Flow through fractures. Water Resourc Res 17:191-199.

Nur A and Byerlee J D (1971) An exact effective stress law for elastic deformation of rock with fluids. J Geophys Res 76:6414-6419.

Perkins T K and Kern L R (1961) Widths of hydraulic fractures. J Pet Tech Sept 1961:937-949.

Poston S.W, and Berg R.R. (1997) Overpressured gas reservoirs. Society of Petroleum Engineers, Richardson, Texas. p. 138.

Pruess K, Xu T, Apps, J and Garcia J (2001) Numerical modeling of aquifer disposal of CO_2. Society of Petroleum Engineers, SPE Paper no 66537.

Pruess K, Oldenburg C and Moridis G (1999) TOUGH2 User's Guide, Version 2.0, Lawrence Berkeley National Laboratory Report LBLN-43134, Berkeley, CA.

Rutqvist J, Wu Y-S, Tsang C-F and Bodvarsson G (2002) A modeling approach for analysis of coupled multiphase fluid flow, heat transfer, and deformation in fractured porous rock. Int. J. Rock Mech. Min. Sci. 39:429-442.

Rutqvist J. and Tsang C.-F. (2002) A study of caprock hydromechanical changes associated with CO2 injection into a brine aquifer. Environmental Geology, 42, 296-305.

Ruqvist J. and Stephansson O. (2003) The role of hydromechanical coupling in fractured rock engineering. Hydrogeology Journal 11:7–40.

Scholz C H (1990) The Mechanics of Earthquakes and Faulting. Cambridge University Press, New York.

Snow D T (1965) A Parallel Plate Model of Fractured Permeable Media. PhD, University of California, Berkeley.

Swan G (1983) Determination of stiffness and other properties from roughness measurements. Rock Mech and Rock Engng 16:19-38.

Talbot C J and Sirat M (2001) Stress control of hydraulic conductivity in fractured-saturated Swedish bedrock. Engineering Geology 61:145-153.

Terzaghi, K. (1923) Die Berechnung der Durchlässigkeitziffer des Tonesaus dem Verlauf der hydrodynamischen Spannungserscheinungen, Akad. Der Wissenschaften in Wien, Sitzungsberichte, Mathematisch-naturwissenschafttliche Klasse, Part IIa 142(3/4), 125-138.

van Genuchten M.T. (1980) A closed-form equation for predicting the hydraulic conductivity of unsaturated soils. Soil Sci Soc Am J 44: 892-898.

Wang H.F (2000) Theory of linear poroeasticity, Princeton Univ. Press, 287p.

Walsh J B (1981) Effects of pore pressure and confining pressure on fracture permeability. Int. J. Rock Mech. Min. Sci. & Geomech. Abstr. 18:429-435.

Witherspoon P A, Amick C H, Gale J E and Iwai K (1979) Observations of a potential size effect in experimental determination of the hydraulic properties of fractures. Water Resourc Res 15:1142-1146.

Witherspoon P A, Wang J S Y, Iwai K and Gale J E (1980) Validity of cubic law for fluid flow in a deformable rock fracture. Water Resourc Res 16:1016-1024.

Yamamoto K., and Takahashi K. (2004) Importance of geomechanics for the safety of CO_2 geological sequestration. In Ohnishi Y. and Aoki K Eds, Proc. of the ISRM International Symposium: Third Asian Rock Mechanics Symposium, Kyoto, Japan, Nov 30 – Dec 2, 2004, 467–472.

Table 1. Material properties used in TOUGH-FLAC simulations.

Property	Upper	Cap	Aquifer	Basement	Fracture zone
Young's modulus, E (GPa)	5	5	5	5	2.5
Poisson's ratio, ν (-)	0.25	0.25	0.25	0.25	0.25
Biot's parameter, α (-)	1	1	1	1	1
Saturated rock density, ρ_s (kg/m^3)	2260	2260	2260	2260	2260
Zero stress (flowing) porosity, ϕ_0 (-)	0.1	0.01	0.1	0.01	0.1
Residual (flowing) porosity, ϕ_r (-)	0.09	0.009	0.09	0.009	0.05
Zero stress permeability, k_0, (m^2)	1×10^{-15}	1×10^{-17}	1×10^{-13}	1×10^{-17}	1×10^{-12}
Corey (1954) irreducible gas saturation, S_{rg} (-)	0.05	0.05	0.05	0.05	0.05
Corey (1954) irreducible liquid saturation, S_{rl}	0.3	0.3	0.3	0.3	0.3
van Genuchten (1980), P_0 (kPa) (at zero stress)	196	3100	19.6	3100	1
van Genuchten (1980) exponent, m	0.457	0.457	0.457	0.457	0.457

Table 2. Initial conditions in the most important geological formations before CO_2 injection. Values are given as a range because they vary with depth in each formation.

Parameter	Caprock	Aquifer	Fracture zone (closed)
Temperature, T (°C)	40-42.5	42.5-47.5	40-42.5
Pressure, P (MPa)	12.1-13.1	13.1-15.1	12.1-13.1
Mean stress, σ'_M (MPa)	26.6-28.8	28.8-33.2	26.6-28.8
Porosity, ϕ (-)	0.0094	0.094	0.045-0.047
Permeability, k (m^2)	0.3×10^{-17}	0.3×10^{-13}	$0.3\text{-}0.4\times10^{-17}$
van-Genuchten's air-entry pressure, P_0 (kPa)	5800	36.8	5800

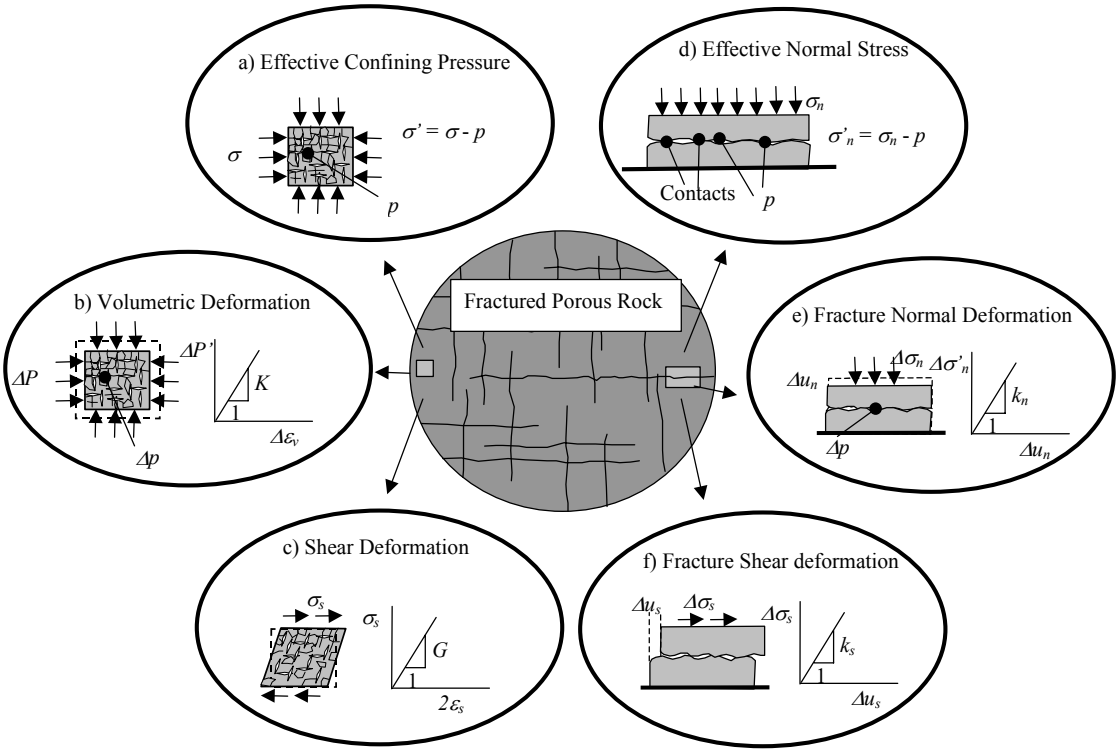

Figure 1. Schematic overview of rock-mechanical processes in a fractured geological media, relevant for caprock integrity (from Rutqvist and Stephansson, 2003).

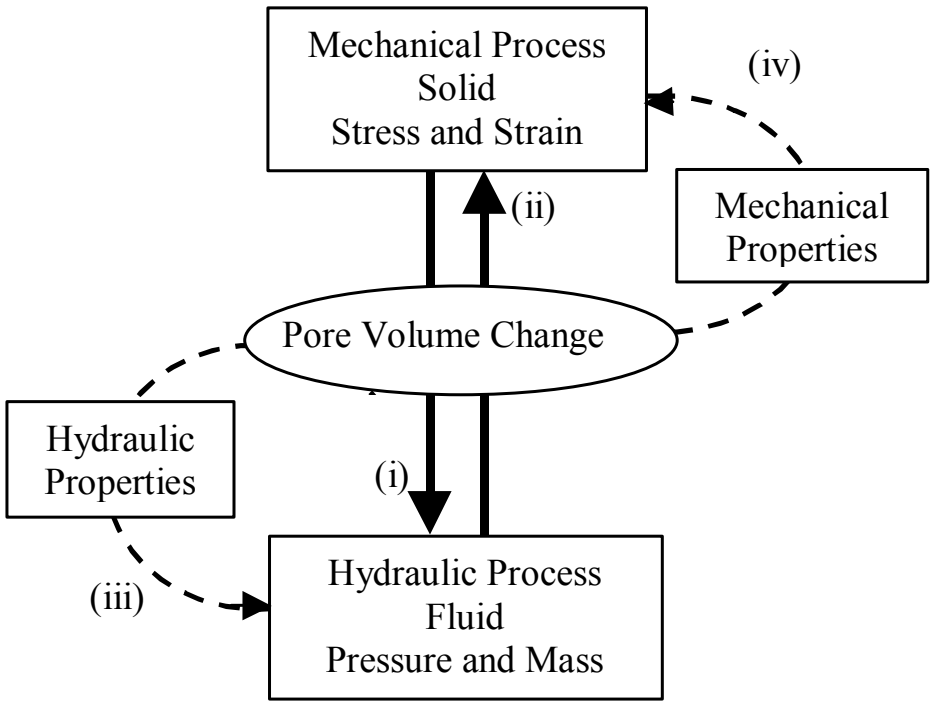

Figure 2. Hydromechanical couplings in geogical media. (i) and (ii) are direct couplings through pore volume interactions, while (iii) and (iv) are indirect couplings through changes in material properties (from Rutqvist and Stephansson, 2003).

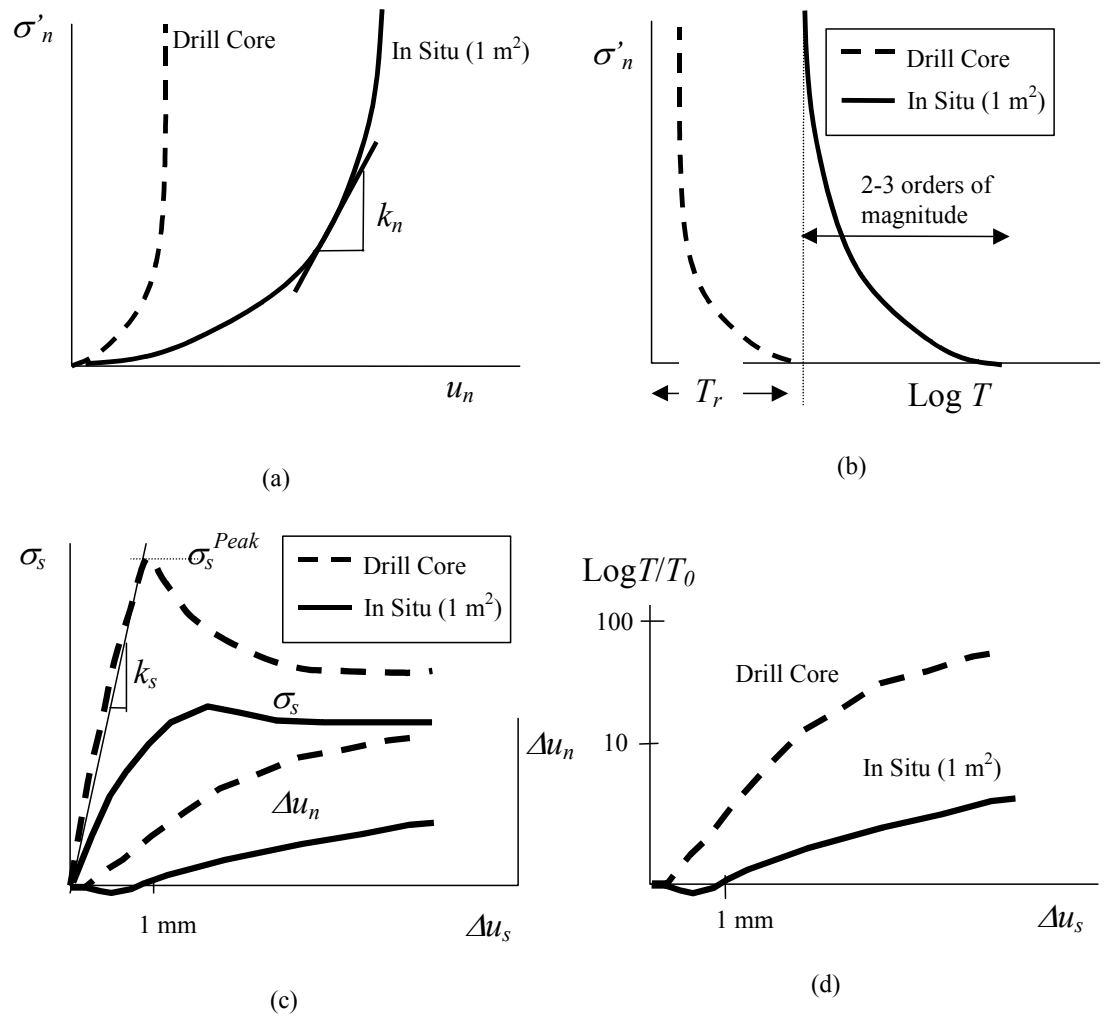

Figure 3. Typical mechanical and hydromechanical fracture responses under normal closure (a and b) and shear (c and d). Effects of sample size is indicated with the laboratory sample response (dashed lines) compared to *in situ* fracture response (1 m^2 size) (modified from Rutqvist and Stephansson, 2003).

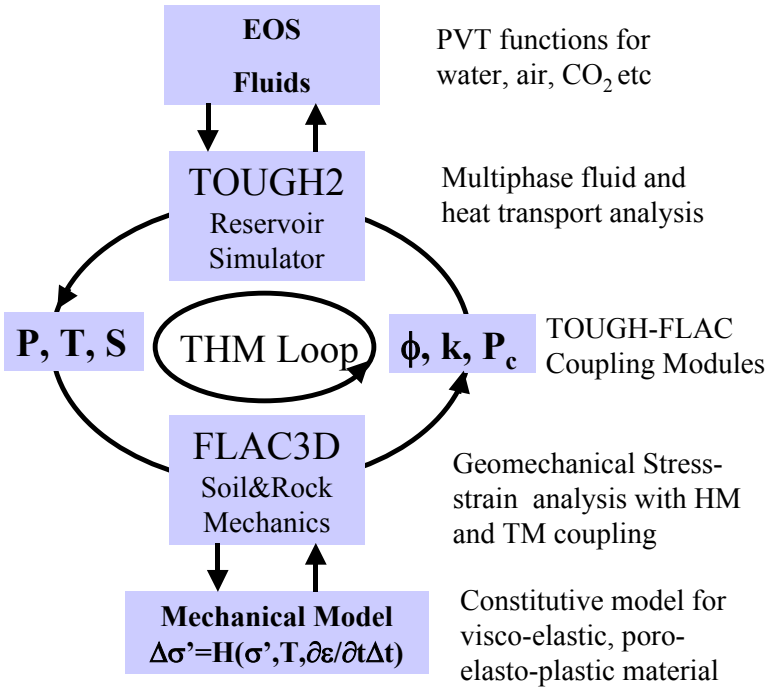

Figure 4. Schematic links between TOUGH2 and FLAC3D for a coupled THM simulation within each time step.

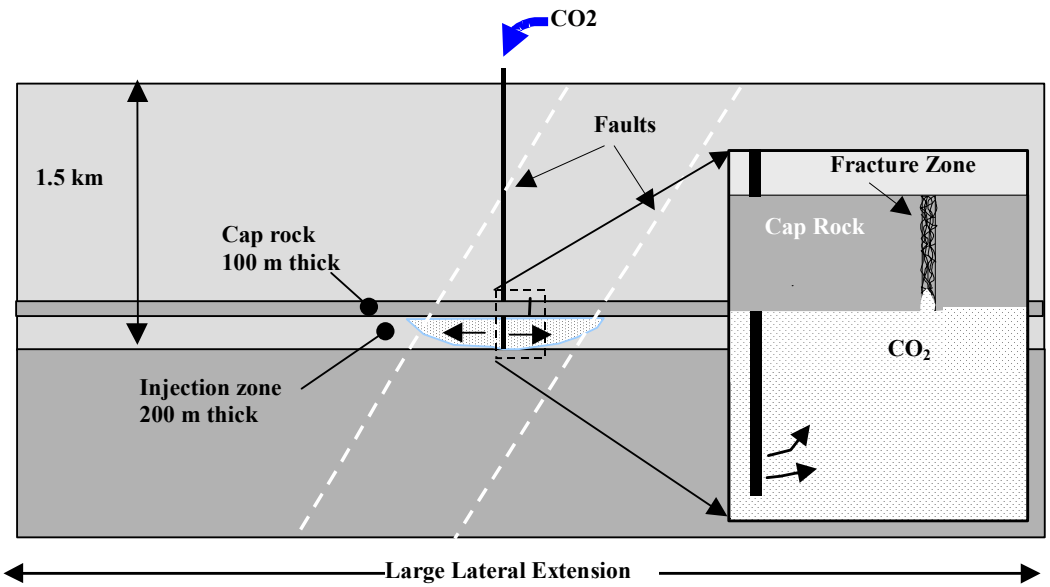

Figure 5. Geometry of simulation cases for CO_2 injection.

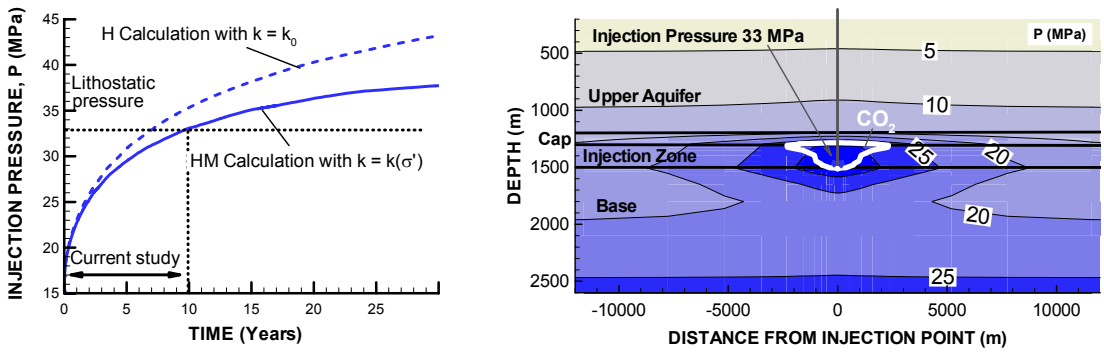

Figure 6. TOUGH-FLAC simulation of CO_2 injection into a caprock/reservoir system with a homogeneous caprock and no laterally sealing faults: (a) Injection pressure versus time, and (b) spread of CO_2 (white line) and fluid pressure distribution after 10 years of injection

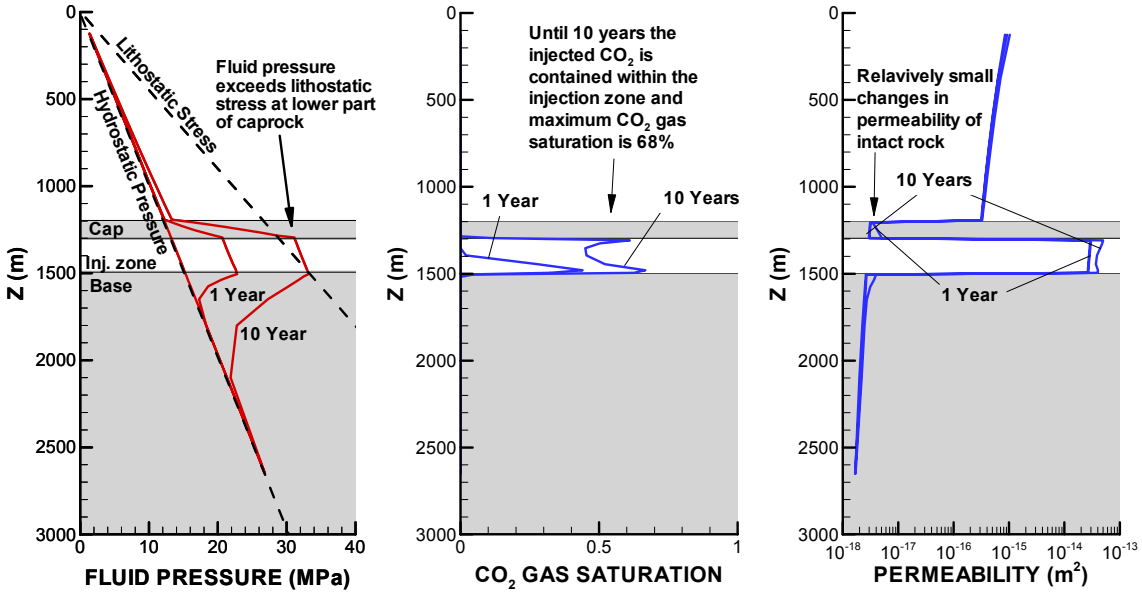

Figure 7. Vertical profiles of fluid pressure, CO_2 gas saturation, and permeability at t = 0, 1 and 10 years.

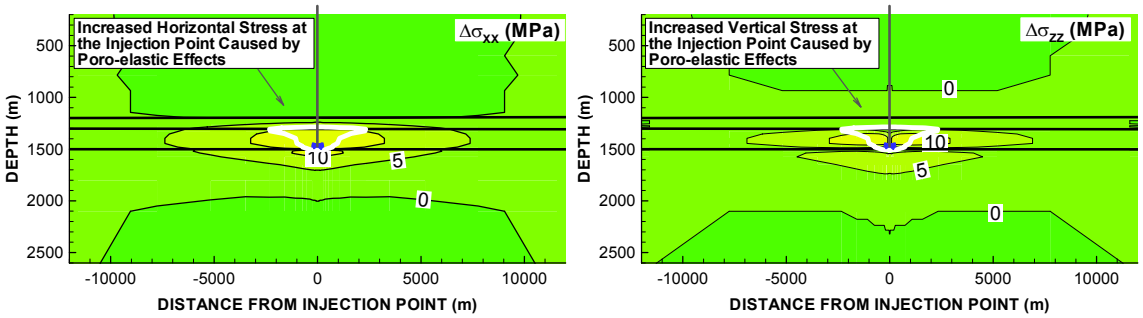

Figure 8. Calculated changes in total *in situ* stresses after 10 years of injection. Extent of CO_2 is shown as a white line.

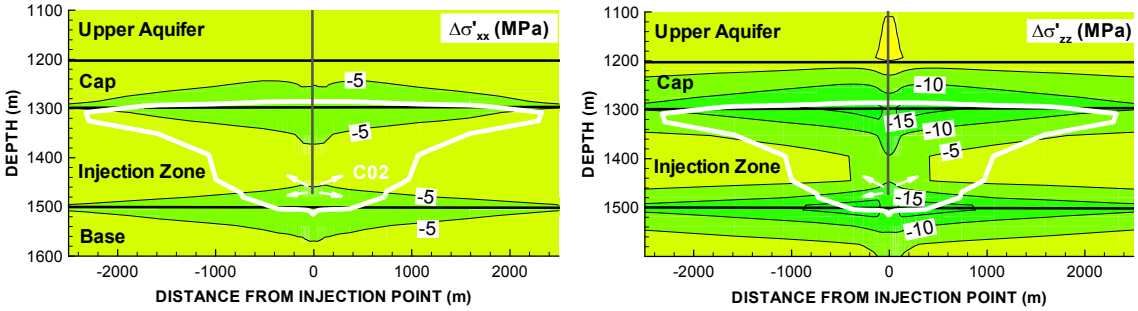

Figure 9. Calculated changes in effective stress in the aquifer-cap rock system after 10 years of CO_2 injection. Light pressure contours indicates where highest stress reduction occurs and the extent of CO_2 is shown as a white line.

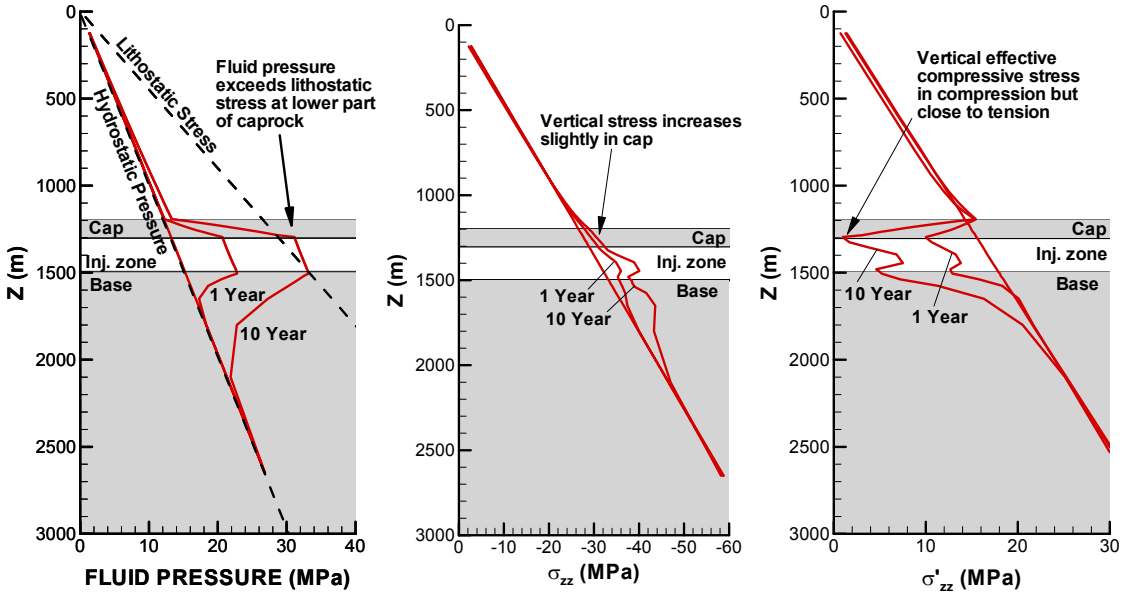

Figure 10. Vertical profiles of fluid pressure, total *in situ* stress and effective vertical stress at t = 0, 1, and 10 years.

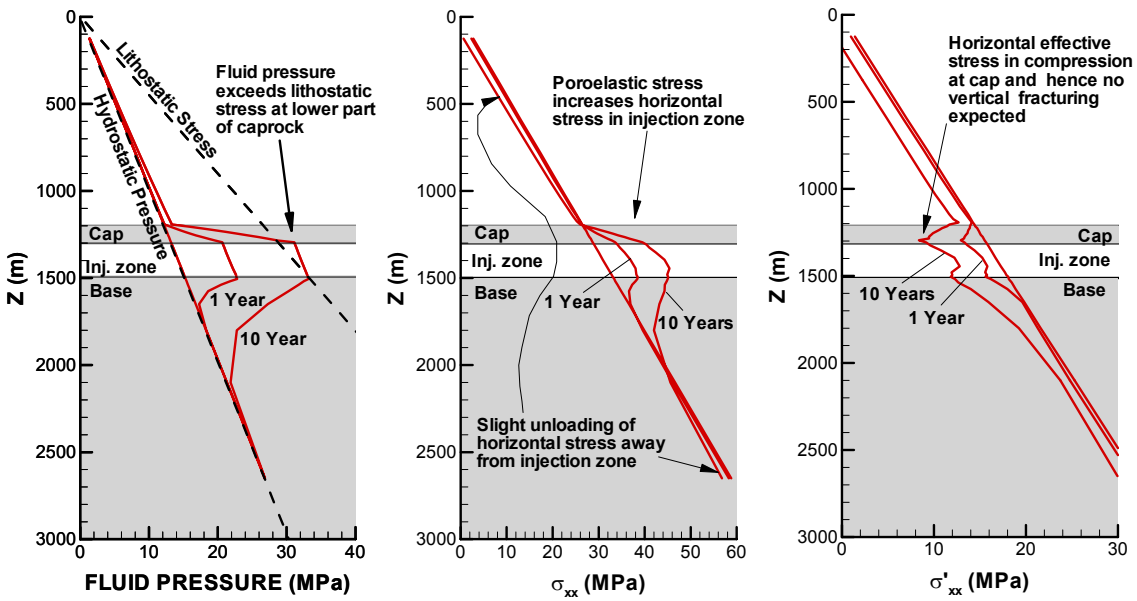

Figure 11. Vertical profiles of fluid pressure, total *in situ* stress and effective horizontal stress at t = 0, 1, and 10 years for isotropic stress regimes ($\sigma_{xxi} = \sigma_{zzi}$)

.

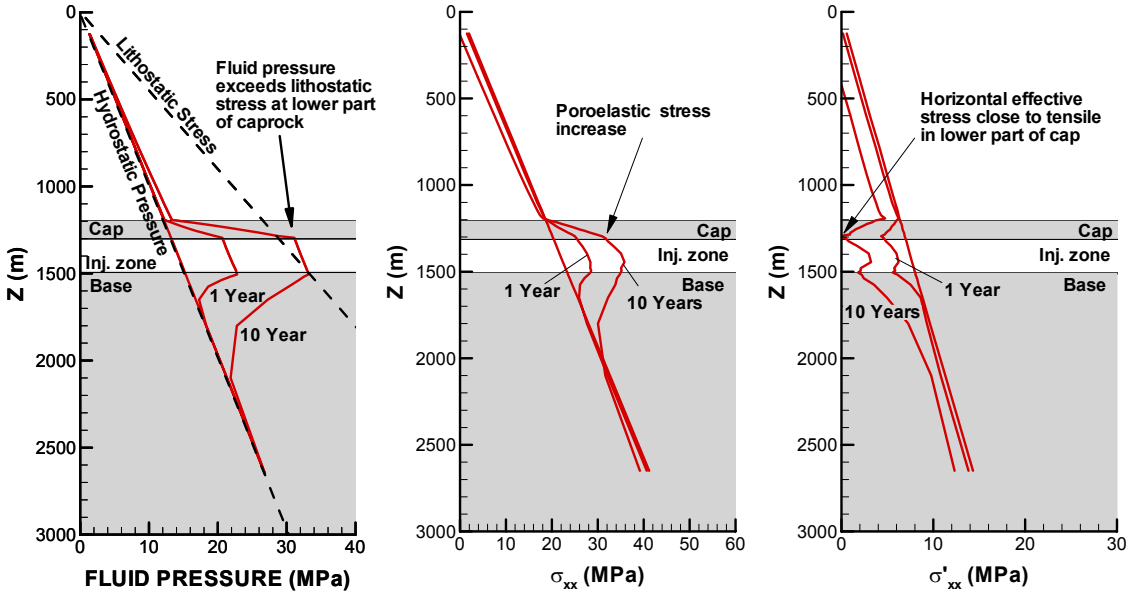

(b) Reverse faulting stress regime

Figure 12. Vertical profiles of fluid pressure, total *in situ* stress and effective horizontal stress at t = 0, 1, and 10 years for reverse faulting stress regimes ($\sigma_{xxi} = 0.7\sigma_{zzi}$).

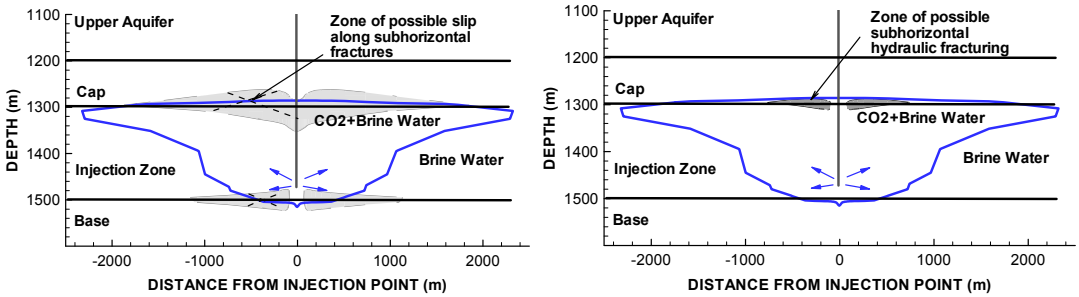

Figure 13. Calculated zones (shaded) of possible shear slip and hydraulic fracturing after 10 years of injection for the case of isotropic stress regime ($\sigma_h = \sigma_v$). The black line shows extent of CO_2.

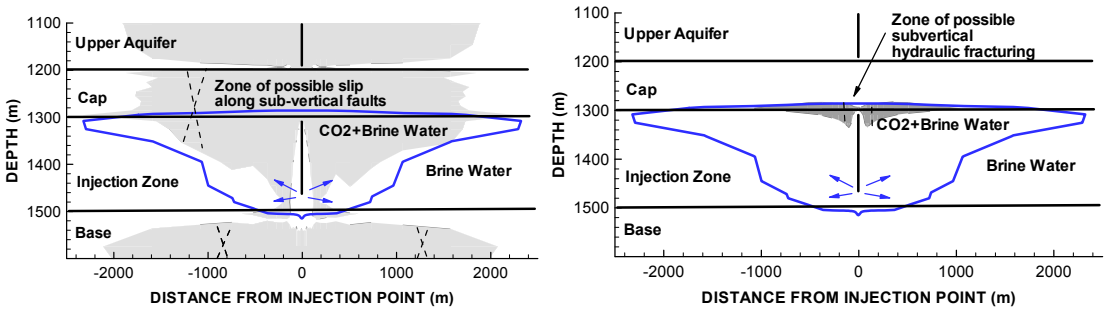

Figure 14. Calculated zones (shaded) of possible shear slip and hydraulic fracturing after 10 years of injection for the case of reverse faulting stress regime ($\sigma_h = 0.7\sigma_v$). The black line shows extent of CO_2.

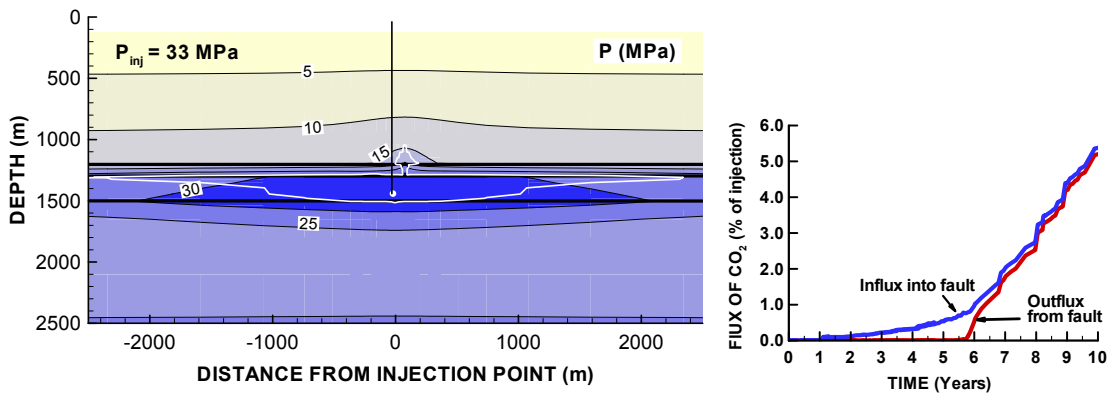

Figure 15. Fluid pressure distribution (left) after 10 years of injection for case of vertical fracture zone in caprock, and CO_2 mass flux into the bottom and out of top of the fracture zone (right) as a function of time.

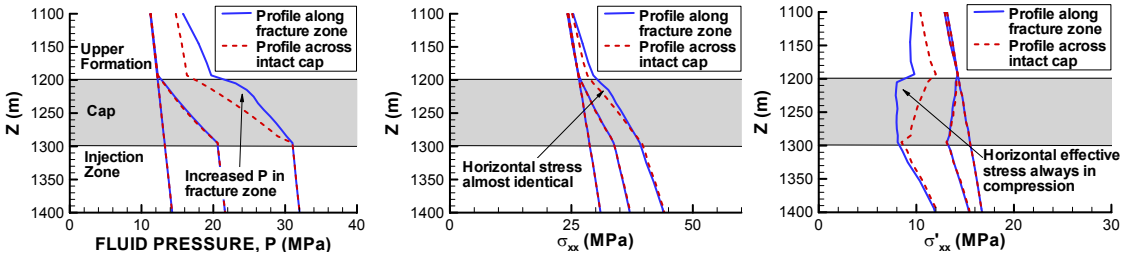

(a) Isotropic stress regime ($\sigma_{xxi} = \sigma_{zzi}$)

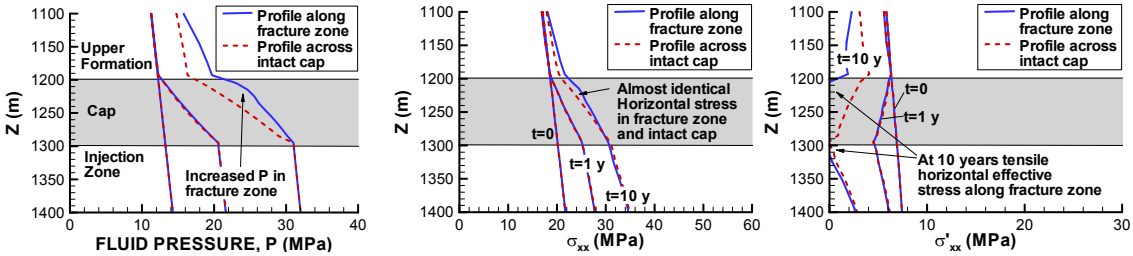

(b) Reverse faulting stress regime ($\sigma_{xxi} = 0.7\sigma_{zzi}$)

Figure 16. Vertical profiles of fluid pressure, total *in situ* stress and effective horizontal stress at t = 0, 1, and 10 years across intact caprock (at x = - 75 m) and along vertical fracture zone (at x = +75 m) for istotropic and reverse faulting stress regimes.

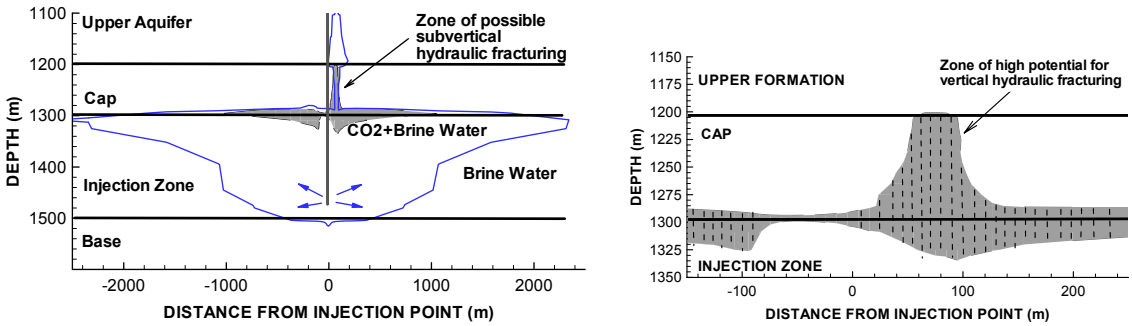

Figure 17. Calculated zone of possible hydraulic fracturing for the case of a pre-existing fracture zone and a reverse faulting stress regime ($\sigma_h = 0.7\sigma_v$). Right figure shows a zoomed in version of the left figure.

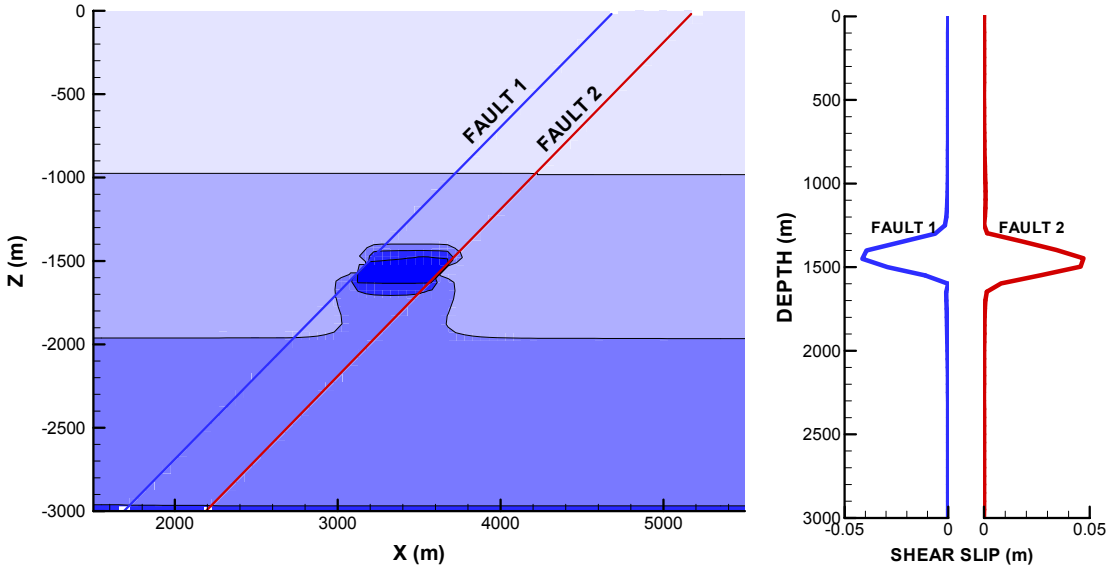

Figure 18. TOUGH–FLAC simulation of fault slip during CO_2 injection into a brine formation sealed by two faults: (a) model with calculated pressure contours, where darker contours represent higher pressure, and (b) calculated shear slip along the two faults.